Solvent Dependence on Cooperative Vibrational Strong Coupling and Cavity Catalysis

*Jaibir Singh, Jyoti Lather and Jino George**

Department of Chemical Sciences, Indian Institute of Science Education and Research (IISER) Mohali, Punjab-140306, India.

ABSTRACT. Strong light-matter coupling offers a unique way to control chemical reactions at the molecular level. Here, we try to compare the solvent effect on a solvolysis process under cooperative vibrational strong coupling (VSC). Two solvents, ethyl acetate and cyclopentanone are chosen to study cavity catalysis by coupling the C=O stretching band of the reactant and the solvent molecules to a Fabry-Perot cavity mode. Interestingly, both the solvent system catalyze the chemical reaction under cooperative VSC conditions. However, the resonance effect on catalysis is observed at different temperatures for the two solvent systems, which is further confirmed by thermodynamic studies. Cavity detuning and other control experiments suggest that cooperative VSC of the solvent plays a crucial role in modifying the transition state energy of the reaction. These findings, along with other observations, cement the concept of polaritonic chemistry.

TOC GRAPHICS

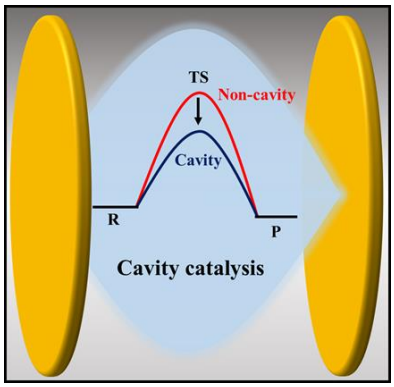

KEYWORDS: Polaritonic chemistry, vibro-polaritonic states, light-matter hybrid states, reaction rate control, vacuum field catalysis.

Strong light-matter coupling and the formation of hybrid states has the potential to alter the chemical and physical properties of the coupled system. Recent experiments on molecular strong coupling suggest that chemical reaction rate can be modified by coupling a vibrational band to an infrared cavity photon.[1–5] The formation of vibropolaritonic states reshuffles the chemical reaction landscape, thereby affecting the reaction dynamics (*a.k.a.* polaritonic chemistry). Polaritonic chemistry is distinctly different from earlier efforts on chemical reaction control using resonant and non-resonant laser experiments. In coherent chemistry, laser excitation injects a large amount of energy into a chemical bond and softens it, thereby achieving a selective bond breaking.[6–8] Nevertheless, the efficiency of bond breaking is poor as the energy dissipates into the available vibrational modes through internal vibrational relaxation pathways.[9] In polaritonic chemistry, a vibrational transition is collectively coupled to a cavity photon (or virtual photon) that internally dresses the molecular state with the electromagnetic field. This is a microscopic phenomenon that

can affect the associated properties such as entropy and coherence.[10,11] This quantum electrodynamics (QED) approach is unique because one can control a chemical process without an external source.[12,13]

The first attempt in this direction was on a photoisomerization reaction by coupling the electronically excited state of merocyanine.[14] Here, the strongly coupled system slowed down the conversion process, thereby affecting its photo-stationary state. This experimental observation seeded the idea of VSC and controlling chemical reaction at the molecular level. Shalabney et al. achieved VSC with poly-vinyl acetate in solid-state in a Fabry-Perot (FP) cavity.[15] Similar VSC experiments with polymers and liquids followed [16] [17,18], and these findings set the stage for modifying homogenous chemical reactions under VSC conditions by A. Thomas et al. [19–21] Later, Hirai et al. reported a similar observation in Prins cyclization of a series of aldehydes and ketones by coupling the C=O band of the reacting species.[22]

There are many theoretical studies on the effect of vacuum field coupling on chemical reactions. Flick et al. introduced the concept of QED coupled with time-dependent density functional theory to understand the nature of dressed states.[23,24] These theoretical finding explained the effect of vibronic coupling that control conical intersections of reacting species. Later, Galego et al. observed the collective behaviour of molecular vibrations that can control a photochemical conversion process.[25] Non-equilibrium behaviour and collective nature of the vibro-polaritonic states are further confirmed by molecular dynamic simulations.[26,27] Theoretical studies based on cavity frequency-dependent dynamical caging effect at a single-molecule level suggest a collective and resonance behaviour in strongly coupled systems.[28,29] There are several theoretical attempts to understand the nature of energy/electron transfer processes that could explain the modification of reaction pathways/dynamics in vibro-polaritonic states.[30–35]

Bulk coupling of a vibrational band to cavity mode has its own limitation for practical applications. The vibrational oscillator gets consumed during the reaction, and the effective coupling strength decreases, which can affect the overall reaction rate. If both the solvent and the reactant molecules possess the same vibrational band, it is possible to couple the solvent molecules to the cavity mode (Figure 1a) and then transfer the effects of VSC via intermolecular interactions to the solute. This process is called cooperative VSC, which offers a better control compared to direct coupling of the reactants.[36] W. Ahn et al. reported that the cooperative VSC of the solvent could also decelerate a chemical reaction by coupling the solvent vibrational band.[37] Cooperative VSC has also been shown to be efficient in modifying super-conductivity, ferromagnetism, supramolecular assembly, selective crystallization processes, etc.[38–42] Recent experiments on enzyme activities also suggest the wider applications of cooperative VSC. We have studied this concept extensively to understand the nature of VSC interactions in a simple ester solvolysis process.[43] There are six mechanisms proposed for the conventional ester solvolysis that purely depends upon the reaction conditions. Cooperative VSC of different derivatives of an ester leads to the breaking of the linear- free-energy relationship, suggesting a clear modification of its TS and rerouting the energy flow between the reaction center and the substituents.[44] Current manuscript is a detailed analysis of cavity catalysis experiments by cooperative VSC in two solvent systems. It also addresses the reproducibility issues reported by Wiesehan et al.[45] Many factors such as optical interference in the UV-VIS spectral regime due to FP cavities, pH variation and acid equilibrium of phenol and phenolate, temperature and stability of the cavity, etc. play a crucial role in obtaining ON resonance effect. A detailed thermodynamic analysis is also conducted to substantiate the effect of different solvent systems in cavity catalysis.

Infrared flow-cell cavities are fabricated by sputtering Au (10 nm) mirror on an optically clean BaF_2 window. Two substrates are placed together to form an FP cavity configuration, as shown in Figure 1b. A mylar spacer (18 μm) defines the path length and thereby fixes the standing wave frequency generated inside the FP cavity. The empty cavity was characterized using an FTIR spectrophotometer, the free spectral range (FSR) is measured carefully to see the stability of the mirrors before injecting the reaction mixture. Repeating the FSR measurements of the empty cavity at regular intervals confirms the cavity's stability before injecting the sample (at least for 30 minutes). Here, we back-calculate the ON/OFF resonance frequency by taking the ratio of empty cavity FSR and the effective refractive index of the medium. We calculate the FSR by averaging at least four higher-order modes in the non-absorbing region (5000 - 7000 cm^{-1}) and estimate the actual cavity mode position at the region of interest. Temperature and humidity for all the experiments are monitored and kept constant throughout the investigation. In order to study the cooperative VSC experiments, we have chosen three different derivatives of an ester as potential candidates. *para*-nitrophenylacetate (PNPA)-a well studies system-is chosen as the model compound with a very strong C=O stretching band at 1761 cm^{-1}. Similarly, 3-methyl- *para*-nitrophenylbenzoate (PNPB) is chosen to have a close by C=O stretching band (1738 cm^{-1}) which has a common leaving group upon solvolysis (Scheme 1). Bis-(2, 4-dinitrophenyl) oxalate (DNPO) is taken as a control (1791 cm^{-1}) to monitor the experiments in the absence of cooperative VSC conditions. All the compounds show very high oscillator strength for the C=O stretching band compared to other available vibrational transitions (Figure 2a). Ester solvolysis process is normally initiated through the activation of the C=O bond, and is chosen as the reaction coordinate in a concerted process. Our previous studies on PNPA and PNPB suggest that cooperative VSC can

control the chemical reaction rate by coupling the C=O stretching band of the reactant and solvent molecules.[36, 44]

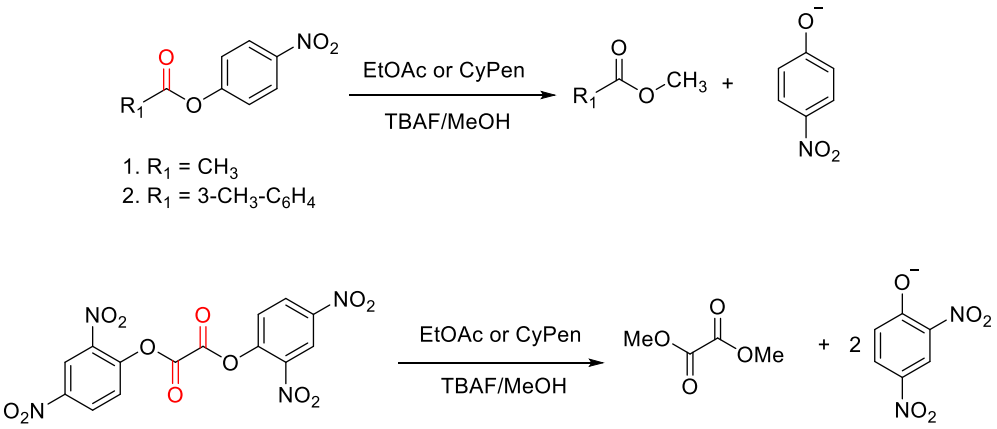

Scheme 1. Scheme for transesterification reaction of three substrates: PNPA, PNPB, and DNPO used for cavity catalysis experiments.

Further, we considered two solvents- ethyl acetate (EtOAc) and cyclopentanone (CyPen)-for cooperative VSC experiments. EtOAc shows a very strong C=O stretching band at 1743 cm^{-1}, as shown in Figure 2b. Similarly, CyPen shows a distinct band at 1748 cm^{-1} which covers the C=O vibrational band of the substrate molecules (PNPA and PNPB). Both the solvent shows the same splitting energy with similar vibro-polaritonic features. Pure EtOAc and CyPen show full-width half-maxima (FWHM) of $\Gamma_{EtOAc} = 32\ cm^{-1}$ and $\Gamma_{CyPen} = 35\ cm^{-1}$, respectively. An empty cavity shows an FWHM of $\Gamma_c = 32\ cm^{-1}$ for the 9th mode position with a Q-factor of 75 (Figure S1). The vibro-polaritonic states formed at the ON resonance condition gives a Rabi splitting energy of 144 cm^{-1} i.e. much larger than the strong coupling limit ($\frac{\Gamma_{EtOAc}+\Gamma_c}{2} = 32\ cm^{-1}$), indicating that the system is entered into strong coupling regime. This observation is again confirmed by dispersion measurements, as shown in Figures 2c and 2d. Please note that the FWHM of the vibro-polaritonic states formed from EtOAc and CyPen are the same ($\Gamma_{VP+} =$

$21\ cm^{-1}$; $\Gamma_{VP-} = 16\ cm^{-1}$), indicating a similar cooperative VSC condition in the two solvent systems (Figures 2b, S2, and S3).

BaF_2 window (optically transparent from 200 nm to 10 μm) based FP cavities allow us to measure the kinetic traces in the UV-VIS region while monitoring the vibro-polaritonic states. For PNPA and PNPB substrates, *para*-nitrophenoxide (PNP^-) ions are formed as the product, which shows an absorption envelope with a maximum at 400 nm (Figure S4). PNP^- formed in the reaction is in equilibrium with *para*-nitrophenol which complicates the rate calculation. The equilibrium constant changes with time due to pH variation as the solvolysis reaction progresses. This forces us to follow the initial rate, assuming a pseudo-first-order fit (for more details, see section 2; SI). On the other hand, DNPO solvolysis gives 2,4-dinitrophenoxide that shows a distinct absorption maximum at 292 nm. During the optimization process, we control the flatness of the mirrors by observing the Newton rings formed at the center of the cavity. Centering the Newton ring into the middle position helps us to place an aperture (approx. 4 mm), thereby fixing the probing area for both IR and UV-VIS spectroscopic measurements. Temporal evolution of the PNP^- are collected at regular intervals, and a linear regression fit gives the apparent rate (k_{app}) of the reaction. k_{app} at 298K is calculated for three substrates in non-cavity conditions and averaged for EtOAc and CyPen solvent systems (Table S2). The same stock solution of TBAF is used in the experiments wherever possible; in other cases, at least three sets of non-cavity data are collected to compare the cavity experiments. FSR tuning experiments are done for all the substrates in both solvent systems and plotted as k_{app} *versus* mode position, shown in Figures 3 and S6. Interestingly, the cooperative VSC of PNPA and PNPB in EtOAc show a rate enhancement at the ON resonance condition. The apparent rate is fitted with a Gaussian error curve to understand the nature of cooperative VSC. In EtOAc solvent system, both the substrates show an enhancement maximum

at approx. 1743 cm^{-1}, indicating the involvement of the solvent vibrational band. Population standard deviation (σ± and 2σ±) obtained from the fitting show the mode tuning should be within 12 cm^{-1} to see an enhancement effect at 298K. Kinetic action spectra (detuning experiments) conducted at 298 K for PNPA/CyPen system show a negligible change in the reaction rate (Figure 5). Another notable point is that the DNPO substrate having minimum overlap with the EtOAc solvent system doesn't respond to the tuning experiments. This underlines the effect of cooperative VSC on the solvolysis of esters. Relative errors (±20 %) of the tuning experiments are calculated in CyPen solvent system assuming the rates are not affected under VSC conditions (Figure S6). Strong coupling experiments suggest that the coupling strength is the same for all the substrates in both solvent systems.

Table 1. Thermodynamic parameters for cavity and non-cavity in EtOAc and CyPen solvent systems.

Solvent	***Substrate***	***Non-Cavity***			***Cavity***			
		$\Delta H^{\neq}$ (kJ/mol)	$\Delta S^{\neq}$ (J/Kmol)	$\Delta G^{\neq}$ (kJ/mol)	$\Delta H^{\neq}$ (kJ/mol)	$\Delta S^{\neq}$ (J/Kmol)	$\Delta G^{\neq}$ (kJ/mol)	$\Delta\Delta G^{\neq}$ (kJ/mol)
EtOAc	**PNPA**	70.3	-62.6	89.0	56.3	-101.2	86.5	-2.5
	PNPB	67.7	-84.4	92.9	180.9	308.8	88.8	-4.1
	DNPO	32.7	-189.4	89.1	32.3	-190.2	89.0	-0.1
CyPen	**PNPA**	34.2	-180.1	87.9	96.2	29.0	87.5	-0.4
	PNPB	77.8	-51.4	93.1	114.2	-72.5	92.5	-0.6
	DNPO	58.3	-105.8	89.8	58.0	-107.1	89.9	0.1

Thermodynamic experiments were conducted to understand the origin of the rate modification. Temperature-dependent experiments in cavity and non-cavity conditions are executed in a thermostat with temperatures varying from 20 to 35°C (Figure 4). Cavity data are recorded at ON resonance (with respect to the solvent vibrational band) condition for all the measurements, which

gives a good least-square fitting of Eyring equation to calculate the activation parameters. Interestingly, for PNPA/EtOAc coupled cavity shows $\Delta\Delta G^{\ddagger}$ of -2.5 kJ/mol compared to the non-cavity conditions. Similarly, $\Delta\Delta G^{\ddagger}$ of -4.1 kJ/mol is obtained for PNPB/EtOAc system. Repeating the same experiments in the CyPen solvent system shows a reshuffling of $\Delta H^{\ddagger}$ and $\Delta S^{\ddagger}$ under ON resonance conditions. Interestingly, DNPO in both the solvent systems doesn't respond to cavity coupling (Figure 4 e, f). DNPO control experiments indicate the importance of vibrational energy overlap between the reactant and the solvent molecules (cooperativity) to achieve cavity catalysis. The extracted activation parameters of the cavity and non-cavity systems are tabulated in Table 1.

Thermodynamics experiments suggest that two solvent systems respond differently to VSC. EtOAc solvent system drastically modifies the thermodynamics parameters that lead to a change of $\Delta G^{\ddagger}$ upto 4 kJ/mol at ON resonance, whereas the changes are small in CyPen solvent system. Please note that VSC induced $\Delta\Delta G^{\ddagger}$ is similar to solvation energy change due to solvent polarity variation in conventional chemical reactions.[46] VSC can affect both the standard Gibbs free-energy (ΔG^{0})[47] as well as the activation free-energy ($\Delta G^{\ddagger}$). Here, solvent coordination in the TS may have a major role in controlling the reaction mechanism. For example, it has been proposed that solvent can push PNPA hydrolysis through a concerted pathway. Here, solvent molecules coordinate the TS in such a way that it controls the reaction mechanism.[48] In the current experiment, EtOAc may coordinate to the charged tetrahedral TS much better than CyPen under VSC conditions. This is reflected in the activation free-energy changes in CyPen solvent system. Detuning experiments of PNPA in CyPen at elevated temperature (40 % rate enhancement at 303 K) also support the above statement (Figure 5). Cooperative VSC between the solvent (EtOAc) and the reactant (PNPA and PNPB) molecules may be ordering the vibrational dipoles (similar to dipole field effect) in a better way that can stabilize the TS.[46] The geometry of the solvent may also play a crucial role that can

control the vibrational energy transfer between the reactant and the solvent molecules. The above observations point to the role of solvent organization and its effect on the reaction dynamics under VSC conditions.

In conclusion, we attempted to compare the effect of solvent on a solvolysis process under VSC conditions. Unlike CyPen, EtOAc has a prominent effect in controlling the activation free-energy. This also points to the fact that cooperative VSC is not the only criteria to decide upon the reaction dynamics. The solvent organization in the TS may be the crucial factor that affects the TS geometry and hence the activation free-energy of the coupled system. This again emphasizes the role of available vibrational relaxation pathways and their modification under VSC conditions. Understanding the reaction dynamics of cooperative VSC in solvolysis reactions is a herculean task. However, these experiments may help a step further in understanding the effect of VSC in chemical reactions.

ASSOCIATED CONTENT

Supporting Information. Details of the sample preparation, cavity fabrication, FTIR, and UV-VIS analysis are given in Section 1 of the supporting information. Kinetic rate approximation, temporal evolution spectra, kinetic traces for ON/OFF resonant cavities, and the details of the thermodynamic analysis are also given in the subsequent sections.

AUTHOR INFORMATION

Corresponding Author

*jgeorge@iisermohali.ac.in

Notes

The authors declare no competing financial interests.

ACKNOWLEDGMENT

MoE-Scheme for Transformational and Advanced Research in Sciences (MoE-STARS/STARS-1/175) is acknowledged for funding. J. S. thank Shyama Prasad Mukherjee Fellowship (SPMF) from CSIR, and J. L. thank IISER Mohali for the fellowship. The authors thank the department of chemical sciences, IISER Mohali, for availing research lab facilities.

REFERENCES

1) Garcia-Vidal, F. J.; Ciuti, C.; Ebbesen, T. W. Manipulating Matter by Strong Coupling to Vacuum Fields. *Science* **2021**, *373*.
2) Nagarajan, K.; Thomas, A.; Ebbesen, T. W. Chemistry under Vibrational Strong Coupling. *J. Am. Chem. Soc.* **2021**, *143*, 16877–16889.
3) Hertzog, M.; Wang, M.; Mony, J.; Börjesson, K. Strong Light–Matter Interactions: A New Direction within Chemistry. *Chem. Soc. Rev.* **2019**, *48*, 937–961.
4) Hirai, K.; Hutchison, J. A.; Uji-i, H. Recent Progress in Vibropolaritonic Chemistry. *ChemPlusChem* **2020**, *85*, 1981–1988.
5) Ruggenthaler, M.; Tancogne-Dejean, N.; Flick, J.; Appel, H.; Rubio, A. From a Quantum-Electrodynamical Light–Matter Description to Novel Spectroscopies. *Nat. Rev. Chem.* **2018**, *2*, 0118.
6) Frei, H.; Pimentel, G. C. Selective Vibrational Excitation of the Ethylene-Fluorine Reaction in a Nitrogen Matrix. I. *J. Chem. Phys.* **1983**, *78*, 3698–3712.
7) Brumer, P.; Shapiro, M. *Chemistry: Controlling Chemical Reactions with Lasers. Acc. Chem. Res.* **1989**, *22*, 407–413.

8) Zare, R. N. Laser Control of Chemical Reactions. *Science* **1998**, *279*, 1875–1879.

9) Semparithi, A.; Keshavamurthy, S. Intramolecular Vibrational Energy Redistribution as State Space Diffusion: Classical-Quantum Correspondence. *J. Chem. Phys.* **2006**, *125*, 141101.

10) Scholes, G. D.; DelPo, C. A.; Kudisch, B. Entropy Reorders Polariton States. *J. Phys. Chem. Lett.* **2020**, *11*, 6389–6395.

11) DelPo, C. A.; Kudisch, B.; Park, K. H.; Khan, S.-U.-Z.; Fassioli, F.; Fausti, D.; Rand, B. P.; Scholes, G. D. Polariton Transitions in Femtosecond Transient Absorption Studies of Ultrastrong Light–Molecule Coupling. *J. Phys. Chem. Lett.* **2020**, *11*, 2667–2674.

12) Flick, J.; Ruggenthaler, M.; Appel, H.; Rubio, A. Atoms and Molecules in Cavities, from Weak to Strong Coupling in Quantum-Electrodynamics (QED) Chemistry. *Proc. Natl. Acad. Sci. U. S. A.* **2017**, *114*, 3026–3034.

13) Schwartz, T.; Hutchison, J. A.; Genet, C.; Ebbesen, T. W. Reversible Switching of Ultrastrong Light-Molecule Coupling. *Phys. Rev. Lett.* **2011**, *106*, 196405.

14) Hutchison, J. A.; Schwartz, T.; Genet, C.; Devaux, E.; Ebbesen, T. W. Modifying Chemical Landscapes by Coupling to Vacuum Fields. *Angew. Chem. Int. Ed.* **2012**, *51*, 1592–1596.

15) Shalabney, A.; George, J.; Hutchison, J.; Pupillo, G.; Genet, C.; Ebbesen, T. W. Coherent Coupling of Molecular Resonators with a Microcavity Mode. *Nat. Commun.* **2015**, *6*, 5981.

16) George, J.; Shalabney, A.; Hutchison, J. A.; Genet, C.; Ebbesen, T. W. Liquid-PhaVibrational Strong Coupling. . *J. Phys. Chem. Lett.* **2015**, *6*, 1027–1031.

17) Simpkins, B. S.; Fears, K. P.; Dressick, W. J.; Spann, B. T.; Dunkelberger, A. D.; Owrutsky, J. C. Spanning Strong to Weak Normal Mode Coupling between Vibrational

and Fabry–Pérot Cavity Modes through Tuning of Vibrational Absorption Strength. *ACS Photonics* **2015**, *2*, 1460–1467.

18) Long, J. P.; Simpkins, B. S. Coherent Coupling between a Molecular Vibration and Fabry–Perot Optical Cavity to Give Hybridized States in the Strong Coupling Limit. *ACS Photonics* **2015**, *2*, 130–136.

19) Thomas, A.; George, J.; Shalabney, A.; Dryzhakov, M.; Varma, S. J.; Moran, J.; Chervy, T.; Zhong, X.; Devaux, E.; Genet, C. Ground-state Chemical Reactivity under Vibrational Coupling to the Vacuum Electromagnetic Field. *Angew. Chem.* **2016**, *128*, 11634–11638.

20) Thomas, A.; Lethuillier-Karl, L.; Nagarajan, K.; Vergauwe, R. M. A.; George, J.; Chervy, T.; Shalabney, A.; Devaux, E.; Genet, C.; Moran, J. Tilting a Ground-State Reactivity Landscape by Vibrational Strong Coupling. *Science* **2019**, *363*, 615–619.

21) Thomas, A.; Jayachandran, A.; Lethuillier-Karl, L.; Vergauwe, R. M. A.; Nagarajan, K.; Devaux, E.; Genet, C.; Moran, J.; Ebbesen, T. W. Ground State Chemistry under Vibrational Strong Coupling: Dependence of Thermodynamic Parameters on the Rabi Splitting Energy. *Nanophotonics* **2020**, *9*, 249–255.

22) Hirai, K.; Takeda, R.; Hutchison, J. A.; Uji-i, H. Modulation of Prins Cyclization by Vibrational Strong Coupling. *Angew. Chem.* **2020**, *132*, 5370–5373.

23) Pellegrini, C.; Flick, J.; Tokatly, I. V; Appel, H.; Rubio, A. Optimized Effective Potential for Quantum Electrodynamical Time-Dependent Density Functional Theory. *Phys. Rev. Lett.* **2015**, *115*, 093001.

24) Flick, J.; Rivera, N.; Narang, P. Strong Light-Matter Coupling in Quantum Chemistry and Quantum Photonics. *Nanophotonics* **2018**, *7*, 1479–1501.

25) Galego, J.; Garcia-Vidal, F. J.; Feist, J. Suppressing Photochemical Reactions with Quantized Light Fields. *Nat. Commun.* **2016**, *7*, 13841.

26) Li, T. E.; Nitzan, A.; Subotnik, J. E. Collective Vibrational Strong Coupling Effects on Molecular Vibrational Relaxation and Energy Transfer: Numerical Insights via Cavity Molecular Dynamics Simulations. *Angew. Chem. Int. Ed.* **2021**, *60*, 15533–15540.

27) Li, T. E.; Subotnik, J. E.; Nitzan, A. Cavity Molecular Dynamics Simulations of Liquid Water under Vibrational Ultrastrong Coupling. *Proc. Natl. Acad. Sci. U. S. A.* **2020**, *117*, 18324.

28) Li, X.; Mandal, A.; Huo, P. Cavity Frequency-Dependent Theory for Vibrational Polariton Chemistry. *Nat. Commun.* **2021**, *12*, 1315.

29) Li, X.; Mandal, A.; Huo, P. Theory of Mode-Selective Chemistry through Polaritonic Vibrational Strong Coupling. *J. Phys. Chem. Lett.* **2021**, *12*, 6974–6982.

30) Pino, J. del; Feist, J.; Garcia-Vidal, F. J. Quantum Theory of Collective Strong Coupling of Molecular Vibrations with a Microcavity Mode. *New J. Phys.* **2015**, *17*, 053040.

31) Herrera, F.; Spano, F. C. Cavity-Controlled Chemistry in Molecular Ensembles. *Phys. Rev. Lett.* **2016**, *116*, 238301.

32) Herrera, F.; Owrutsky, J. Molecular Polaritons for Controlling Chemistry with Quantum Optics. *J. Chem. Phys.* **2020**, *152*, 100902.

33) Ribeiro, R. F.; Martínez-Martínez, L. A.; Du, M.; Campos-Gonzalez-Angulo, J.; Yuen-Zhou, J. Polariton Chemistry: Controlling Molecular Dynamics with Optical Cavities. *Chem. Sci.* **2018**, *9*, 6325–6339.

34) Xiang, B.; Ribeiro, R. F.; Du, M.; Chen, L.; Yang, Z.; Wang, J.; Yuen-Zhou, J.; Xiong, W. Intermolecular Vibrational Energy Transfer Enabled by Microcavity Strong Light–Matter Coupling. *Science* **2020**, *368*, 665–667.

35) Feist, J.; Garcia-Vidal, F. J. Extraordinary Exciton Conductance Induced by Strong Coupling. *Phys. Rev. Lett.* **2015**, *114*, 196402.

36) Lather, J.; Bhatt, P.; Thomas, A.; Ebbesen, T. W.; George, J. Cavity Catalysis by Cooperative Vibrational Strong Coupling of Reactant and Solvent Molecules. *Angew. Chem. Int. Ed.* **2019**, *58*, 10635–10638.

37) Ahn, W.; Herrera, F.; Simpkins, B. Modification of Urethane Addition Reaction via Vibrational Strong Coupling. ChemRxiv **2022**. Accessed on April 23rd 2022.

38) Thomas, A.; Devaux, E.; Nagarajan, K.; Chervy, T.; Seidel, M.; Hagenmüller, D.; Schütz, S.; Schachenmayer, J.; Genet, C.; Pupillo, G. Exploring Superconductivity under Strong Coupling with the Vacuum Electromagnetic Field. *arXiv preprint arXiv:1911.01459* **2019**. Accessed on April 23rd 2022.

39) Thomas, A.; Devaux, E.; Nagarajan, K.; Rogez, G.; Seidel, M.; Richard, F.; Genet, C.; Drillon, M.; Ebbesen, T. W. Large Enhancement of Ferromagnetism under a Collective Strong Coupling of YBCO Nanoparticles. *Nano. Lett.* **2021**, *21*, 4365–4370.

40) Joseph, K.; Kushida, S.; Smarsly, E.; Ihiawakrim, D.; Thomas, A.; Paravicini-Bagliani, G. L.; Nagarajan, K.; Vergauwe, R.; Devaux, E.; Ersen, O. Supramolecular Assembly of Conjugated Polymers under Vibrational Strong Coupling. *Angew. Chem., Int. Ed.* **2021**, *60*, 19665–19670.

41) Sandeep, K.; Joseph, K.; Gautier, J.; Nagarajan, K.; Sujith, M.; Thomas, K. G.; Ebbesen, T. W. Manipulating the Self-Assembly of Phenyleneethynylenes under Vibrational Strong Coupling. *J. Phys. Chem. Lett.* **2022**, *13*, 1209–1214.

42) Hirai, K.; Ishikawa, H.; Chervy, T.; Hutchison, J. A.; Uji-i, H. Selective Crystallization via Vibrational Strong Coupling. *Chem. Sci.* **2021**, *12*, 11986–11994.

43) Lather, J.; George, J. Improving Enzyme Catalytic Efficiency by Co-Operative Vibrational Strong Coupling of Water. *J. Phys. Chem. Lett.* **2020**, *12*, 379–384.

44) Lather, J.; Thabassum, A. N. K.; Singh, J.; George, J. Cavity Catalysis: Modifying Linear Free-Energy Relationship under Cooperative Vibrational Strong Coupling. *Chem. Sci.* **2022**, *13*, 195–202.

45) Wiesehan, G. D.; Xiong, W. Negligible Rate Enhancement from Reported Cooperative Vibrational Strong Coupling Catalysis. *J. Chem. Phys* **2021**, *155*, 241103.

46) Anslyn, E. V.; Dougherty. D. A. *Modern Physical Organic Chemistry*. 1st ed.; University Science Books, **2006**; pp 441- 445.

47) Pang, Y., Thomas, A., Nagarajan, K., Vergauwe, R. M., Joseph, K., Patrahau, B.; Wang, K.; Genet, C.; Ebbesen, T. W. On the Role of Symmetry in Vibrational Strong Coupling: The Case of Charge-Transfer Complexation. *Angew. Chem. Int. Ed.* **2020**, *59*, 10436–10440.

48) Xie, D.; Zhou, Y.; Xu, D.; Guo, H. Solvent Effect on Concertedness of the Transition State in the Hydrolysis of P-Nitrophenyl Acetate. *Org. Lett.* **2005**, *7*, 2093–2095.

Figures:

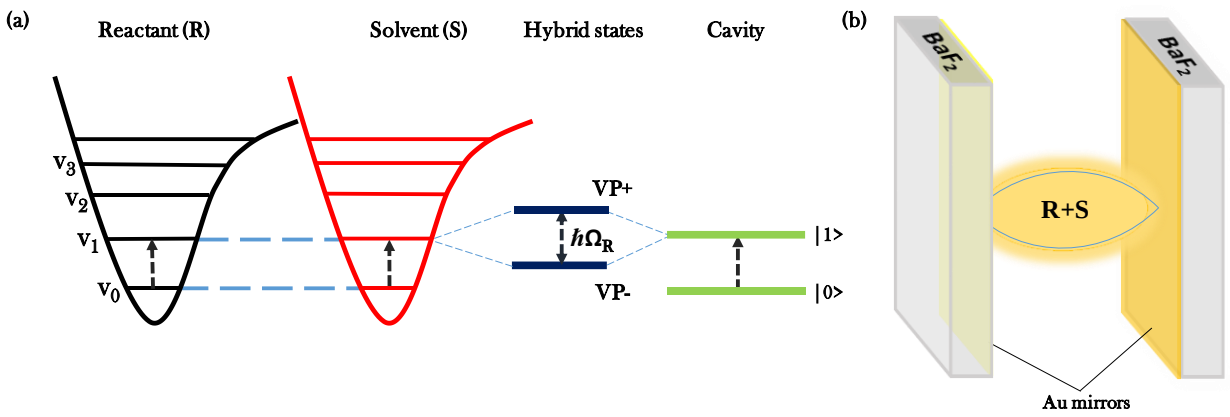

Figure 1. (a) Schematic representation of cooperative vibrational strong coupling and (b) the corresponding Fabry-Perot Cavity configuration used for cavity catalysis.

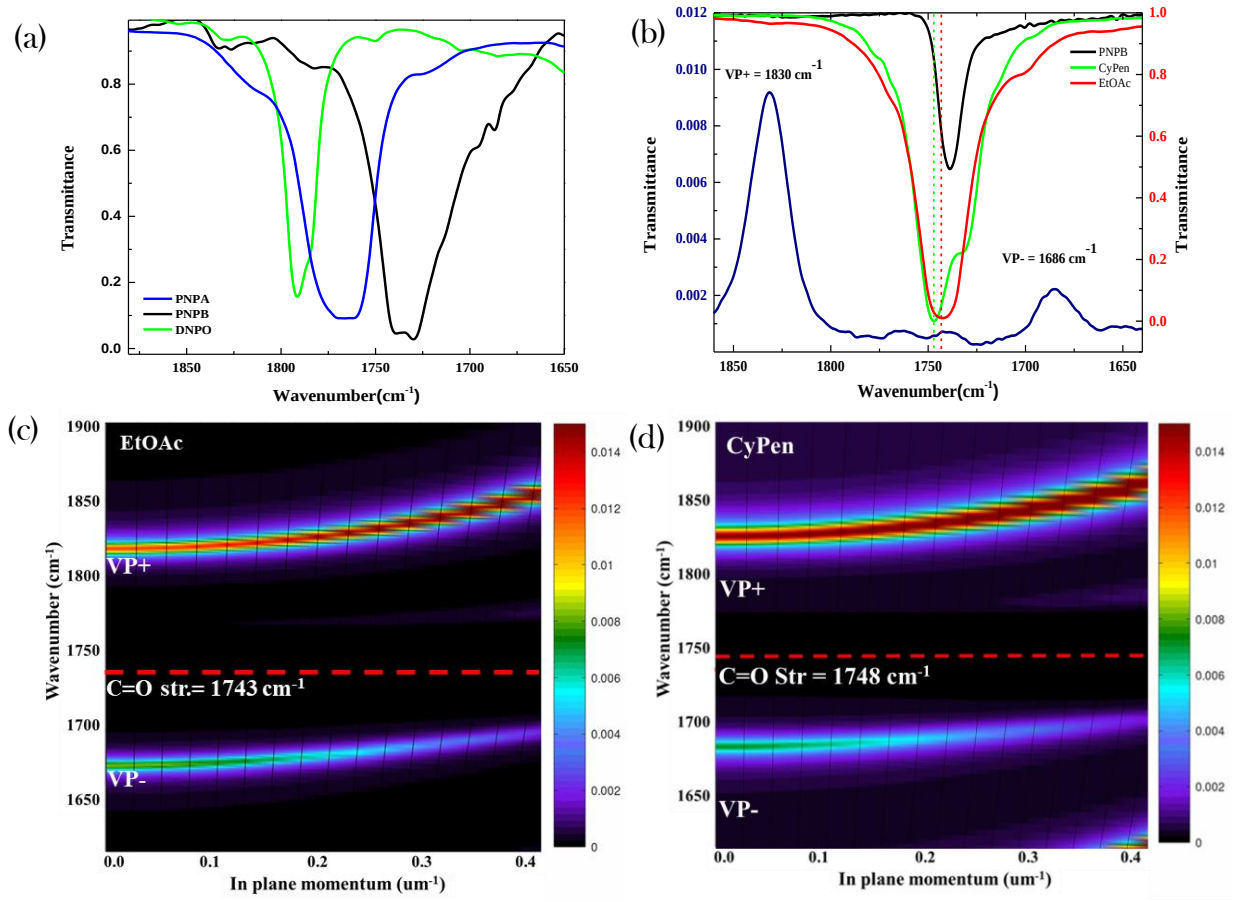

Figure 2. (a) Carbonyl stretching mode of PNPA (blue trace),PNPB (black trace), and DNPO (green trace); (b) VSC of pure ethyl acetate coupled to 9th mode of an F-P cavity, and the corresponding vibro-polaritonic states. TMM simulated dispersion diagram of vibro-polaritonic states formed from (c) ethyl acetate and (d) cyclopentanone.

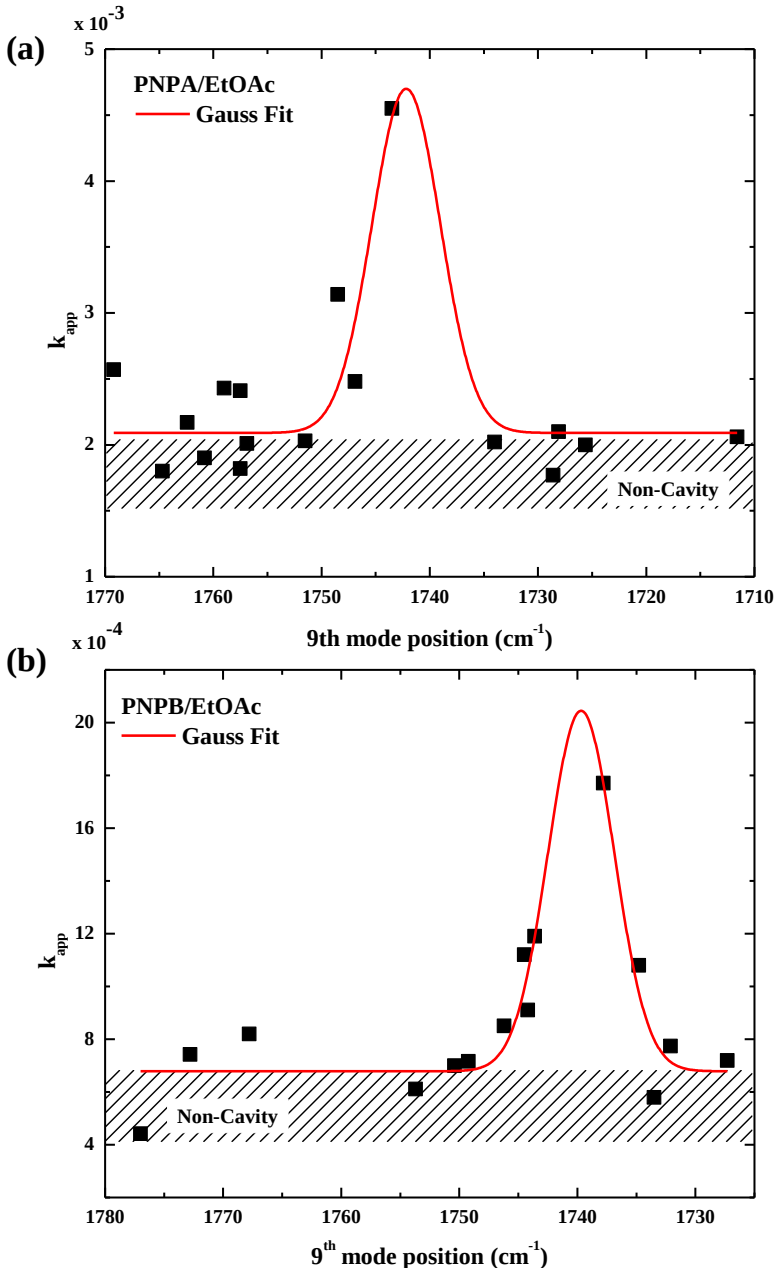

Figure 3. Kinetic action spectra of (a) PNPA, and (b) PNPB in EtOAc solvent system at 298 K. Red line is a Gaussian error fit and the shaded area is the uncertainty in non-cavity kinetic measurements.

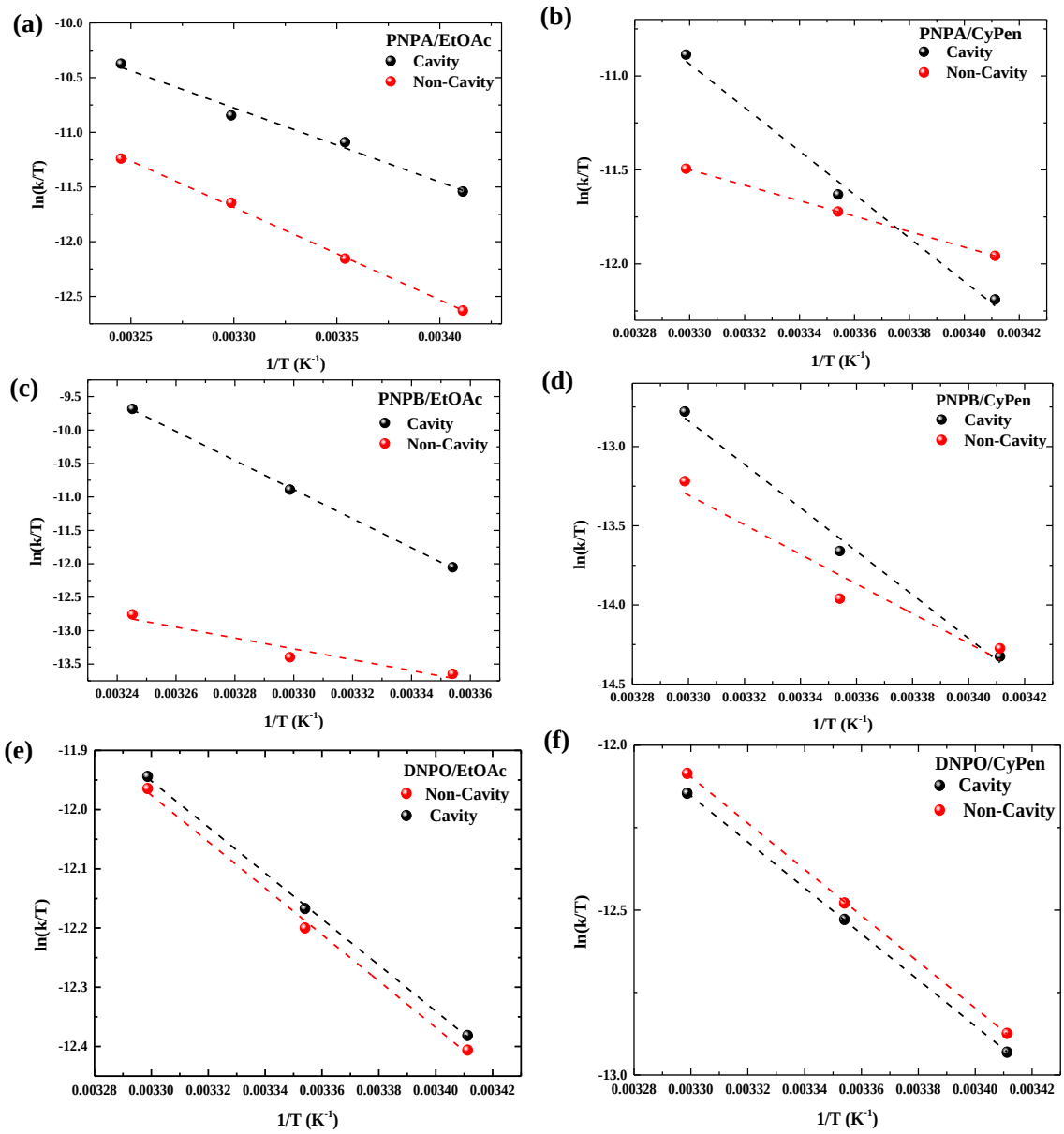

Figure 4. Thermodynamics correlations for cavity (black trace) and non-cavity (red trace) for: PNPA (a), (b); PNPB (c), (d); DNPO (e), (f); in EtOAc (left panel) and CyPen (right panel) solvent systems.

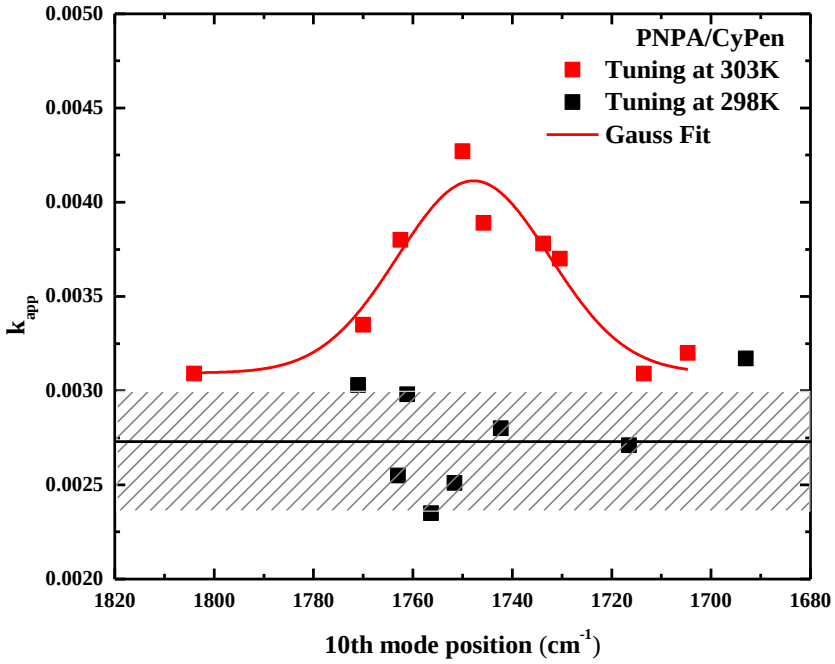

Figure 5. Kinetic action spectra for PNPA (303 K; red dots) and (298 K; black dots) in CyPen. Black line represents the average cavity apparent rate under VSC at 298 K. Red line is a Gaussian error fit.

Supporting Information

Solvent Dependence on Cooperative Vibrational Strong Coupling and Cavity Catalysis

*Jaibir Singh, Jyoti Lather and Jino George**

Department of Chemical Sciences, Indian Institute of Science Education and Research (IISER) Mohali, Punjab-140306, India.

*E-mail: jgeorge@iisermohali.ac.in

CONTENTS:

Section 1:

Materials and methods:

PNPA (p-nitrophenylacetate), DNPO (bis-2,4-dinitrophenyloxalate), TBAF (tetrabutylammonium fluoride), EtOAc (Ethyl acetate), and CyPen (cyclopentanone) were purchased from Merck. PNPB (3-methyl-p-nitrophenylbenzoate) was synthesised in lab following the literature reports.[1]

a) Preparation of stock solutions:

Preparation of TBAF stock solution:

TBAF is a crystalline and hygroscopic compound. 31.5 mg of TBAF was carefully weighed and dissolved in 1 ml methanol (0.1M TBAF) to make a stock solution. Same solution was diluted to 2mM and used.

Preparation of stock solutions of substrates:

18.1 mg PNPA was carefully weighed and dissolved in 1 ml of EtOAc or CyPen to form a 0.1M solution. To prepare a 0.1M solution of PNPB, 27.2 mg PNPB was weighed and dissolved in 1ml of solvent. 4.22mg of DNPO was measured and dissolved in 1 ml of solvent for preparing 0.01M DNPO solution. All the solutions used were kept in a water bath at room temperature before kinetic measurement. 90 ml of the 0.1 M or 0.01M substrate solution was mixed with 10 ml of 0.1M or 2mM TBAF solution respectively to prepare the reaction mixture.

b) Preparation of cavity and non-cavity:

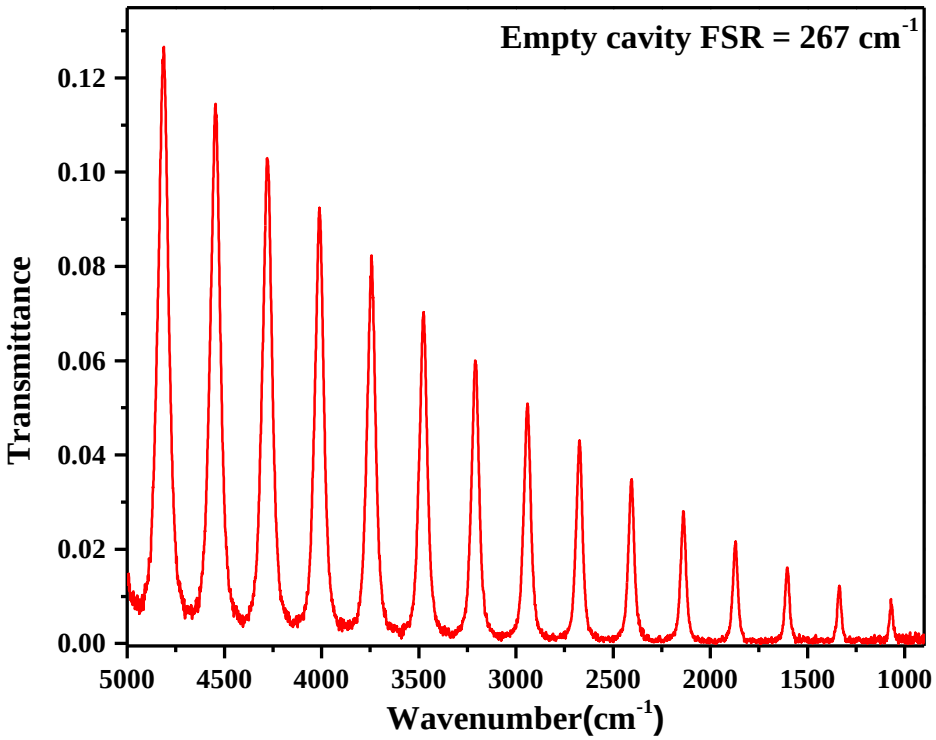

Figure S1. Transmission spectrum of empty Fabry-Perot cavity having free spectral range of 267 cm^{-1}.

Fabry-Perot cavity was prepared by placing two Au mirror sputtered on BaF_2 windows facing one another in a demountable flow cell (Spacac.inc). Spacing between the mirrors was maintained by placing a mylar spacer of 18 mm. Cavity was tuned for different mode positions by loosening or tightening the four screws of the demountable cell. The prepared empty Fabry-Perot cavity was then placed inside an FT-IR spectrophotometer (Bruker INVENIO-R) to see and analyse the formed cavity modes (Figure S1). For non-cavity experiments BaF_2 windows without Au mirrors were used. Reaction mixture was then injected into the cavity resulting in the formation of vibro-polaritons (Figures S2 and S3). Both the solution found to give same coupling strength of 144 cm^{-1} at on-resonance.

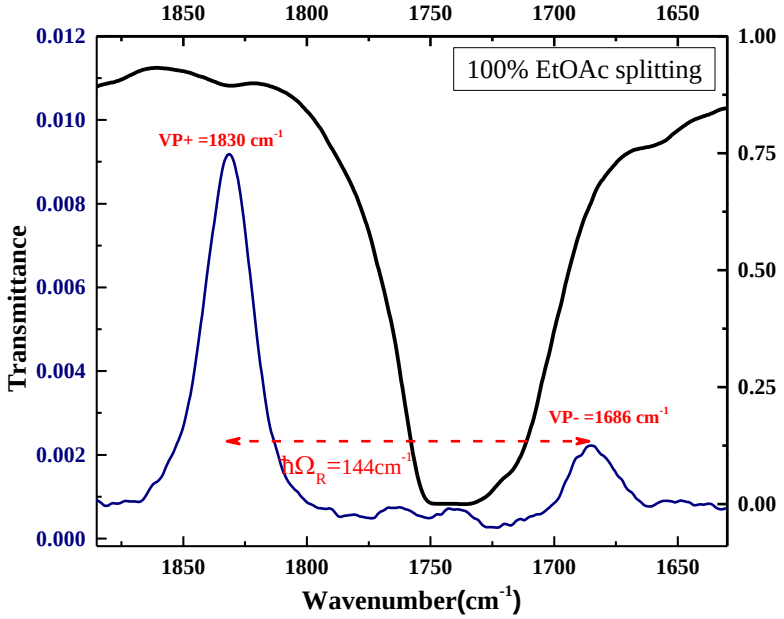

Figure S2. Transmission spectra of 100% EtOAc in non-cavity (black trace) and cavity condition (blue trace).

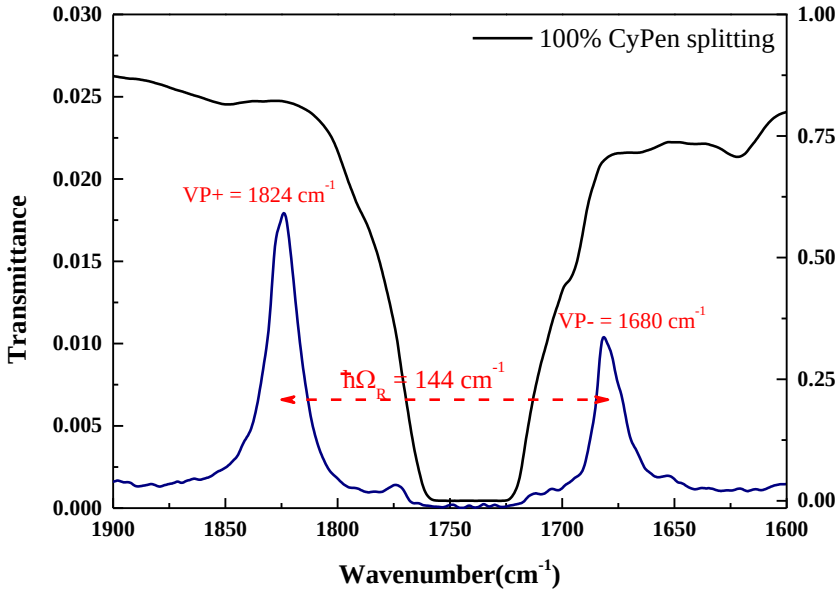

Figure S3. Transmission spectra of 100% CyPen in non-cavity (black trace) and cavity condition (blue trace).

Transfer Matrix Method (TMM) Simulation:

TMM is used for the calculation of the propagation of light through the layers of different refractive indexes. Reflection of light from the single interface between two different mediums is described using the Fresnel equations and extended for multilayer systems. Fabry-Perot cavities also contain stacks of different refractive indexes, TMM is widely used for the simulation of their interference pattern. In the experimental cavity condition, Au coated mirrors of ~10 nm thickness were separated by the layer for reacting solution of the refractive index of 1.37 (for ethyl acetate) and 1.43 (for cyclopentanone). Here, we coupled the 9th cavity mode for ethyl acetate (EtOAc) and the 10th cavity mode for cyclopentanone (CyPen) with the C=O stretching vibration of the respective solvent. For the TMM simulation, we used precisely the same conditions and compared the experimental Rabi splitting with the calculations. Further, the optimised simulation parameters were then used to extract the dispersion plots of Vibro-polaritonic states (used in Figures 2c and 2d).

Section 2: Kinetic rate approximation:

2A) Effects of pH variation:

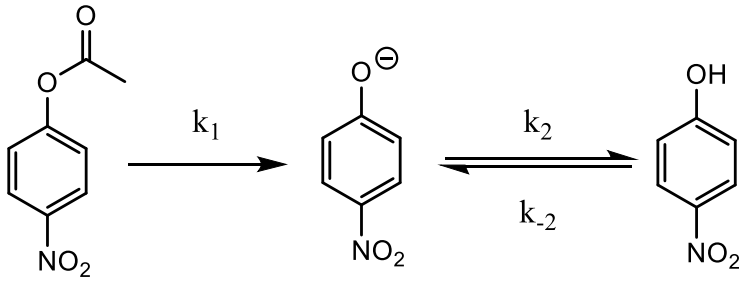

p-nitrophenoxide formed in the above reaction is in equilibrium with p-nitrophenol. The equilibrium between these two species depends on the pH of the solution due to different ionisation. Previous studies suggests that *p-nitrophenol* absrbs at ~317 and *p-nitrophenoxide* show a maximum at ~400 nm. Average pKa of *p-nitrophenol* is 6.99. At pH 8.0, the extinction coefficient of *p-nitrophenoxide* is nearly 9.5 times greater than that of phenol. [2,3] To study the reaction, the pH should not change significantly while acquiring the kinetic traces. pH measurement was conducted for the bulk reaction mixture at every two minutes interval, till 10 minutes to see the trend (Table S1). Here, we maintained the 9: 1 ratio of PNPA: TBAF (400 µl of 0.1M TBAF added to 3600 µl of 0.1M PNPA), similar to cavity coupling conditions. It was observed that the pH variation is still within the basic regime for the initial time, which encouraged us to follow the initial rate calculations. Apparent rate for cavity and non-cavity conditions are plotted using pseudo first-order kinetic fit. Here, we assume that the pH change is negligible and the *p-nitrophenoxide* absorption contribute mostly in the rate calculation.

Table S1: Variation of the pH in the bulk reaction.

Time (Minutes)	pH
0	8.74
2	8.61
4	8.34
6	8.21
8	8.13
10	8.08

2B) Kinetics model for rate approximation at constant pH:

A = 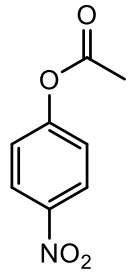

B = 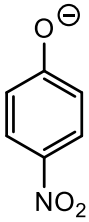

C = 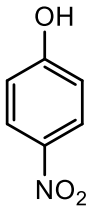

The kinetic rate constant for the above reaction was derived as follows:

$$A \xrightarrow{k_1} B \underset{k_{-2}}{\overset{k_2}{\rightleftharpoons}} C$$

$$A_0 = A + B + C \qquad\qquad K = \frac{C}{B} = \frac{k_2}{k_{-2}}$$

where, K is equilibrium constant.

$$A_0 = A + B + KB$$

$$\Longrightarrow \qquad \boxed{B = \frac{A_0 - A}{K+1}}$$

Similarly

$$\boxed{C = \frac{K(A_0 - A)}{K+1}}$$

$$\frac{dB}{dt} = k_1 A + k_{-2} C - k_2 B$$

$$\frac{dB}{dt} = k_1 A + k_{-2}\left(\frac{K(A_0 - A)}{K+1}\right) - k_2\left(\frac{A_0 - A}{K+1}\right)$$

$$\frac{dB}{dt} = \left(k_1 - \frac{k_{-2}K}{K+1} + \frac{k_2}{K+1}\right)A + \left(\frac{k_{-2}K}{K+1} - \frac{k_2}{K+1}\right)A_0$$

$$\boxed{\frac{dB}{dt} = k'A + constant}$$

Kinetic experiments done in cavity and non-cavity conditions uses initial rate method to extract the apparent rate of the solvolysis process. This method will only give the k_1 value assuming that the reaction is following a pseudo-first-order process.

Section 3: Kinetic experiments

To extract the apparent kinetic rates under the non-cavity and cavity condition, the reaction mixture containing microfluidic cell/cavity was placed into the UV-VIS spectrophotometer (PerkinElmer Lambda 465). Formation of the product was monitored by taking spectrum at regular intervals. For PNPA and PNPB 400nm and for DNPO and 292nm was used to extract the pseudo first-order rate constant. Temporal evolution spectra, and the corresponding linear regression fitting and the calculated apparent rates can be found in Figures S4 and S5.

1. PNPA/EtOAc

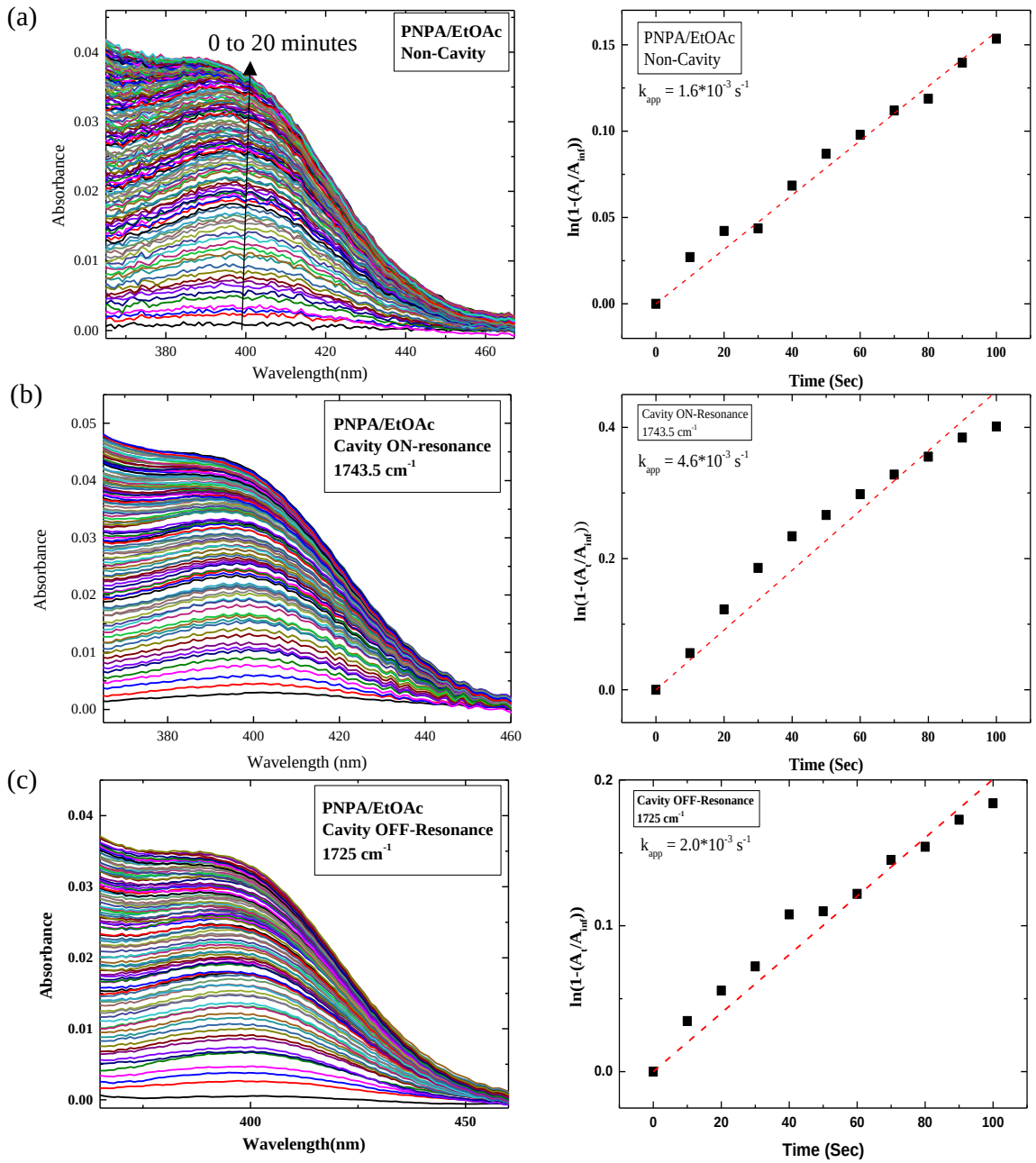

Figure S4. Temporal evolution and the corresponding linear regression fit of kinetic traces: (a) non-cavity, (b) on-resonance cavity, and (c) off-resonance cavity in PNPA/EtOAc system. All the data points are smoothened (50 points) to avoid cavity fringes.

2. PNPB/EtOAc

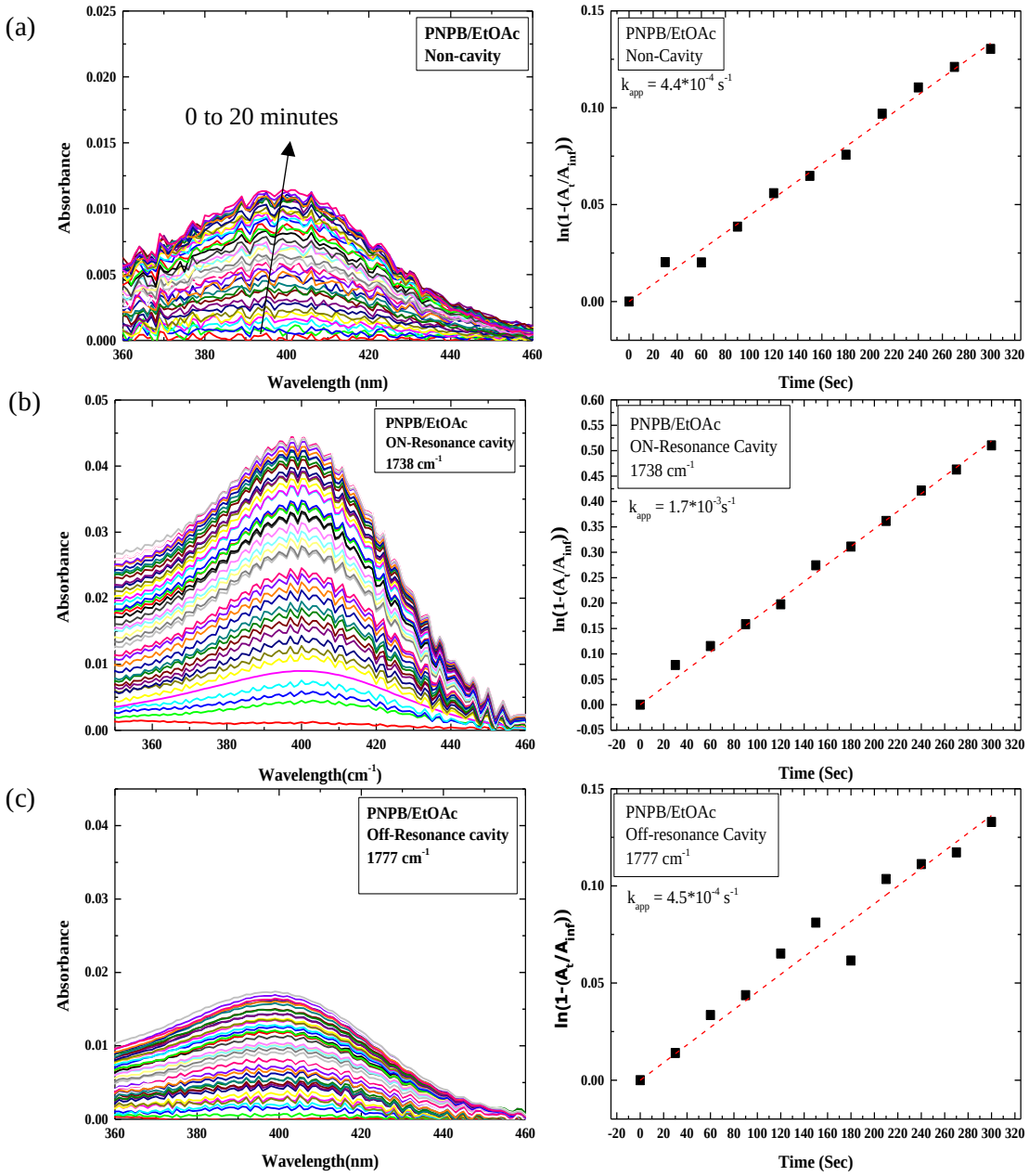

Figure S5. Temporal evolution and the corresponding linear regression fit of kinetic traces: (a) non-cavity, (b) on-resonance cavity, and (c) off-resonance cavity in PNPB/EtOAc system. All the data points are smoothened (50 points) to avoid cavity fringes.

Table S2. Apparent kinetic rate measured at 298 K for cavity and non-cavity in EtOAc and CyPen solvent systems.

Sl. No.	*Substrate*	*EtOAc*		*CyPen*	
		Non-Cavity (s^{-1})	Cavity (s^{-1})	Non-Cavity (s^{-1})	Cavity (s^{-1})
1.	PNPA	$1.8*10^{-3}$	$4.5*10^{-3}$	$2.4*10^{-3}$	$2.7*10^{-3}$
2.	PNPB	$4.4*10^{-4}$	$17.7*10^{-4}$	$3.5*10^{-4}$	$3.5*10^{-4}$
3.	DNPO	$1.5*10^{-3}$	$1.6*10^{-3}$	$1.1*10^{-3}$	$1.1*10^{-3}$

Section 4: Thermodynamic calculations

We calculated the thermodynamics parameters by measuring the apparent rate constant at different temperatures and then fitting them into the Eyring equation. Please note that the cavity ON condition is 1743 cm^{-1} and 1748 cm^{-1} for EtOAc and CyPen solvent systems, respectively.

The Eyring equation used in Figure 4 and Table 1 in the main text is as follows:

$$k_{app} = \frac{k_b T}{h} \exp\left(-\frac{\Delta H^{\neq}}{RT} + \frac{\Delta S^{\neq}}{R}\right)$$

1. PNPA/EtOAc:

Non-Cavity:

$-\frac{\Delta H^{\neq}}{R}$ = - 8457.25 (slope)

$ln\frac{k_b}{h} + \frac{\Delta S^{\neq}}{R}$ = 16.22 (intercept)

$\Delta H^{\neq}$ = 70.3 kJ /mol

$\Delta S^{\neq}$ = (16.22 – 23.75) ×8.314

$\Delta S^{\neq}$ = - 62.6 J/K.mol

$\Delta G^{\neq} = \Delta H^{\neq} - T\Delta S^{\neq}$

= 70.3 – 298.15×(-62.6)

$\Delta G^{\neq}$ =89.0 kJ/mol

Cavity:

$-\frac{\Delta H^{\neq}}{R}$ = - 6774.52(slope)

$ln\frac{k_b}{h} + \frac{\Delta S^{\neq}}{R}$ = 11.58 (intercept)

$\Delta H^{\neq}$ = 56.3 kJ /mol

$\Delta S^{\neq}$ = (11.58 – 23.75) ×8.314

$\Delta S^{\neq}$ = - 101.2 J/K.mol

$\Delta G^{\neq} = \Delta H^{\neq} - T\Delta S^{\neq}$

= 56.32 – 298.15×(-101.2)

$\Delta G^{\neq}$ = 86.5 kJ/mol

$\Delta\Delta G^{\neq}$ = 86.5 – 89.0 = - 2.5 kJ/mol

2. PNPB/EtOAc

Non-Cavity:

$-\frac{\Delta H^{\neq}}{R}$ = - 8141.48 (slope)

$ln\frac{k_b}{h} + \frac{\Delta S^{\neq}}{R}$ = 13.59 (intercept)

$\Delta H^{\neq}$ = 67.7 kJ /mol

$\Delta S^{\neq}$ = (13.59 – 23.75) ×8.314

$\Delta S^{\neq}$ =- 84.4 J/K.mol

$\Delta G^{\neq} = \Delta H^{\neq} - T\Delta S^{\neq}$

= 67.69 – 298.15×(-84.4)

$\Delta G^{\neq}$ = 92.9 kJ/mol

Cavity:

$-\frac{\Delta H^{\neq}}{R}$ = - 21758.02 (slope)

$ln\frac{k_b}{h} + \frac{\Delta S^{\neq}}{R}$ = 60.89 (intercept)

$$\mathbf{\Delta H^{\neq} = 180.8\ kJ\ /mol}$$

$\Delta S^{\neq} = (60.89 - 23.75) \times 8.314$

$$\mathbf{\Delta S^{\neq} = 308.8\ J/K.mol}$$

$\Delta G^{\neq} = \Delta H^{\neq} - T\Delta S^{\neq}$

$= 60.89 - 298.15 \times (-308.8) = 88.8$ kJ/mol

$$\mathbf{\Delta G^{\neq} = 88.8\ kJ/mol}$$

$$\mathbf{\Delta\Delta G^{\neq} = 88.8 - 92.9 = -4.1\ kJ/mol}$$

Section 5: Tuning Experiments:

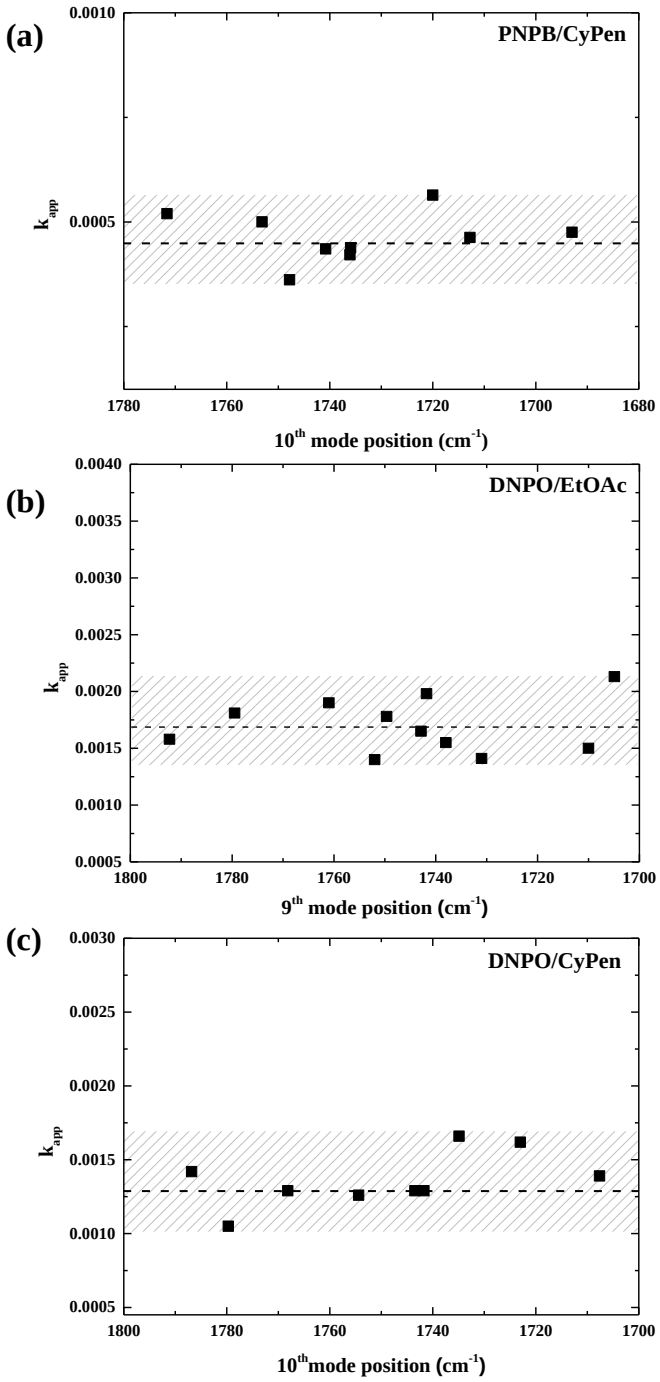

Figure S6: Tuning experiments a) PNPB/CyPen, b) DNPO/EtOAc, c) DNPO/CyPen at 298 K.

Reference:

1. Lather, J.; Thabassum, A. N. K.; Singh, J.; George, J., Cavity catalysis: modifying linear free-energy relationship under cooperative vibrational strong coupling. *Chem. Sci.* **2022,** *13*, 195-202.
2. Biggs, A. I. (1954). A spectrophotometric determination of the dissociation constants of p-nitrophenol and papaverine. *Transactions of the Faraday Society*, *50*(0), 800–802.

3. Peng, Y., Fu, S., Liu, H., & Lucia, L. A. (2016). Accurately Determining Esterase Activity via the Isosbestic Point of p-Nitrophenol. *BioResources; Vol 11, No 4 (2016)*.